separations

MDPI

Article

Numerical Modeling and Analysis of Harvesting Atmospheric Water Using Porous Materials

Sadeem S. Alkinani [1], Mohamed F. El-Amin [1,2,*] and Tayeb Brahimi [1]

[1] Energy Research Lab, College of Engineering, Effat University, Jeddah 21478, Saudi Arabia
[2] Mathematics Department, Faculty of Science, Aswan University, Aswan 81528, Egypt
* Correspondence: momousa@effatuniversity.edu.sa

Abstract: Nowadays, harvesting water from the atmosphere is becoming a new alternative for generating fresh water. To the author's best knowledge, no mathematical model has been established to describe the process of harvesting water from the atmosphere using porous materials. This research seeks to develop a new mathematical model for water moisture absorption in porous materials to simulate and assess harvesting atmospheric water. The mathematical model consists of a set of governing partial differential equations, including mass conservation equation, momentum equation, associated parameterizations, and initial/boundary conditions. Moreover, the model represents a two-phase fluid flow that contains phase-change gas–liquid physics. A dataset has been collected from the literature containing five porous materials that have been experimentally used in water generation from the air. The five porous materials include copper chloride, copper sulfate, magnesium sulfate, manganese oxides, and crystallites of lithium bromide. A group of empirical models to relate the relative humidity and water content have been suggested and combined with the governing to close the mathematical system. The mathematical model has been solved numerically for different times, thicknesses, and other critical parameters. A comparison with experimental findings was made to demonstrate the validity of the simulation model. The results show that the proposed mathematical model precisely predicts the water content during the absorption process. In addition, the simulation results show that; during the absorption process, when the depth is smaller, the water content reaches a higher saturation point quickly and at a lower time, i.e., quick process. Finally, the highest average error of the harvesting atmospheric water model is around 1.9% compared to experimental data observed in manganese oxides.

Keywords: atmospheric water; porous material; relative humidity; absorption; mathematical modeling; harvesting atmospheric water

check for updates

Citation: Alkinani, S.S.; El-Amin, M.F.; Brahimi, T. Numerical Modeling and Analysis of Harvesting Atmospheric Water Using Porous Materials. *Separations* **2022**, *9*, 364. https://doi.org/10.3390/separations9110364

Academic Editors: Mohamed Nageeb Rashed and Mohamed Farid Cheira

Received: 27 September 2022
Accepted: 4 November 2022
Published: 10 November 2022

1. Introduction

1.1. Overview

In a world of almost 8 billion people, there is a growing awareness that clean water scarcity is becoming a serious problem. The UN warns that by 2030, 1.6 billion people will lack access to safe drinking water at home. Freshwater is getting more challenging due to increased population, global climate change, and the depletion of local water supplies. According to the United Nations (UN-UNESCO) [1], in 2021, over 45% of the world's population suffered from accessing safely managed sanitation facilities, and over 25% lived in water-stress areas. Even though water covers more than 70% of the Earth's surface, 96.5% [2]. Based on data from Gleick [2], Figure 1, the majority of the world's freshwater is inaccessible to humans; of the 2.53% of fresh water, 68.7% is trapped in glaciers, mainly in the Antarctic areas, 30.1% is found in the ground, and only about 1.24% is fresh water found on the surface, which includes lakes (20.91%), ground ice and permafrost (68.95%), rivers (0.49%), and atmosphere (3%). Moreover, UNICEF [3] anticipated that by 2025, two-thirds of the world's population would be affected by water shortages while all ecosystems

around the globe will suffer much more as a result. With only 2.53% of fresh water on earth, where most of it is locked in glacial ice and snow, scientists have investigated three fundamental techniques for water generation, including groundwater extraction, saltwater desalination, and rainfall collecting. Nowadays, harvesting atmosphere water (HAW) is becoming a new alternative source of freshwater. Unless a sustainable water source can be located and appropriately managed, the world will continue to face significant challenges when water availability is limited and quality is variable.

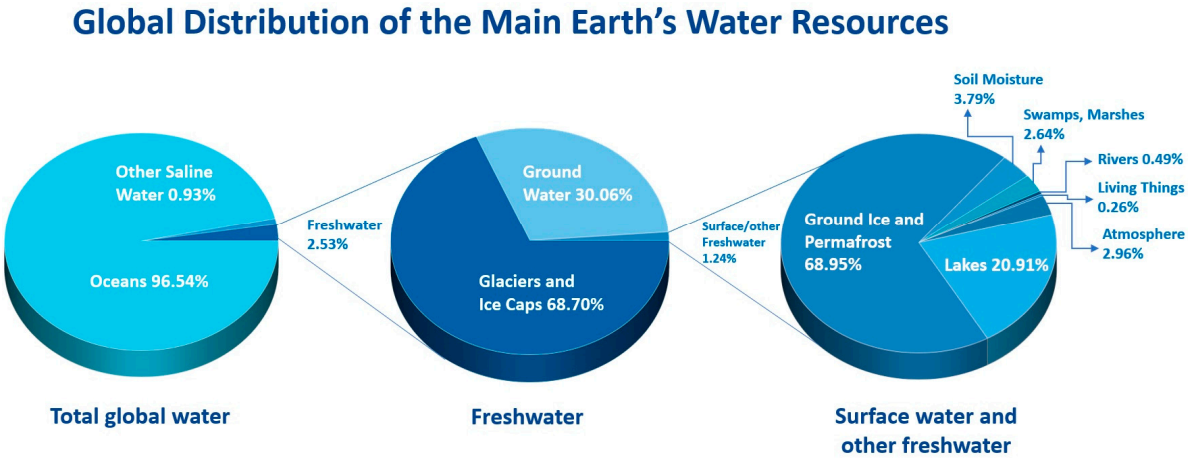

Figure 1. Distribution of Earth's water resources.

Scientists have investigated three fundamental techniques to generate water, including groundwater extraction, saltwater desalination, and rainfall collecting [4,5]. The two major processes used in desalination are membrane process with pressure or electrical-driven technologies such as reverse osmosis (RO), nanofiltration (NF), electrodialysis (ED), electrodialysis reversal (EDR), and thermal processes such as multistage flash distillation (MSF), multi-effect distillation (MED), and vapor compression distillation (VCD) [6,7]. These technologies require a large amount of accessible seawater or brackish water sources, in addition to the effect on the environment and the high operational cost and energy consumption needed for desalination facilities [8]. As a result, desalination does not apply to non-coastal communities that suffer from severe water shortages.

On the other hand, the ability to extract water from the air is by far the most under-explored unconventional water resource, although 3% out of the 1.2% of surface water exists in the atmosphere, which is more than the amount of freshwater in the rivers (0.49%), as shown in Figure 1. In recent years, significant efforts have been devoted to harvesting water from the atmosphere [5,9,10]. The most apparent manifestations of atmospheric water are clouds floating in the sky, fog near the ground, and water vapor in the air. As shown in Figure 2, harvesting atmospheric water (HAW) uses different methods [4]: fog collection employing mesh nets, condensation-cooling systems, and absorbent materials.

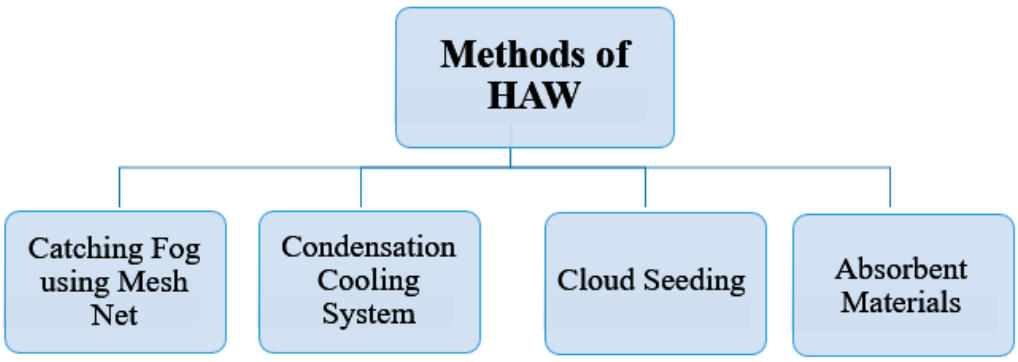

Figure 2. Harvesting atmospheric water methods.

The mesh net is a technology that uses tall towers to gather water from wind-driven fog. When the wind travels through the mesh, freshwater droplets form and drip into an underlying gutter, from which pipes lead the water into the storage and distribution system. It works well in environments with high relative humidity (RH) of 100% [11]. This system is commonly implemented in coastal and mountainous fog-prone areas [12]. Depending on topography and geography, the fog collector uses different train materials such as alloy or plastic. The local community supporters are engaged in harvesting water because it has low maintenance options and supports green technology for drinking water purposes. The fog water collector method entails erecting a rectangular mesh parallel to the wind. The mesh holds the fog droplets as the wind blows high humid air, and as the water droplets become more prominent, they fall into the tank due to gravity.

Drinking water could be obtained from an atmospheric water generator by condensing water vapor in the atmosphere. It employs the thermodynamic cycle, mechanical refrigeration, and modern electrical control [13]. Improvements in technology have been created to boost efficiency and, as a result, reduce energy consumption while increasing water generation. The procedure involves air and water treatments to remove suspended particles in the atmosphere and water-soluble volatile organic compounds, boost water mineralization for drinking water, and maintain optimal conservation for stored water to ensure the highest quality of water [14].

It can be an alternate source of preventing rain enhancement, increasing the volume of water harvesting from the air [15]. The conservative water technology includes the dispersion of small materials into clouds collected as raindrops. It is a particle of raindrops or ice crystals that are transformed into rain or snow and collected as water. Cloud seeding technology supports precipitation of 20% according to the availability of cloud resources [16]. It can add the advantage of cloud water, increasing groundwater through rainfall. The technology helps increase rainfall in dry areas.

Adsorption-based HAW differs from standard HAW systems in that it uses desiccant materials to absorb water vapors from the air and achieves better thermal efficiency [17]. The key benefit is that the desiccant materials may be renewed using solar thermal energy, and the condensation process can occur at room temperature. The desiccant material comes into touch with the ambient air at night and absorbs the water vapors in the first step. The desiccant material is packed into a closed system in the second step, where a substantial quantity of heat is used to regenerate the desiccant material. The material desorbs the water vapors during regeneration, and the collected vapors are condensed into liquid form. The current study focuses on the absorption part (see the schematic diagram in Figure 3). The HAW may be achieved in low relative humidity locations using this method. With a focus on solar-driven hygroscopic water harvesting, Zhuang et al. [18] examined current advancements in atmospheric water collection. The concepts of high adsorption capacity sorbents, heat control, vapor condensation, and water collection were also investigated. Another review paper by Asim et al. [19] discussed the progress in sorbent materials, condensation, and system design, considering functionalization and composites when modifying the sorbent materials. It is crucial to research sorbents' stability and life cycle, water absorption, adsorption kinetics, heat and mass transport, regeneration conditions, water-collecting surface design, and system design. Metal-organic frameworks (MOFs) have been considered to be efficient AWH adsorbents. They can supply water in high and low relative humidity [20]. A high-efficiency AWH system with hygroscopic PPy-Cl, a hydrophilic network of poly-NIPAM, and hydrophilicity switching based on the poly-NIPAM was developed by Zhao et al. [21] Effective water transport along the interconnecting networks of functional polymers enables these synergistic functionalities.

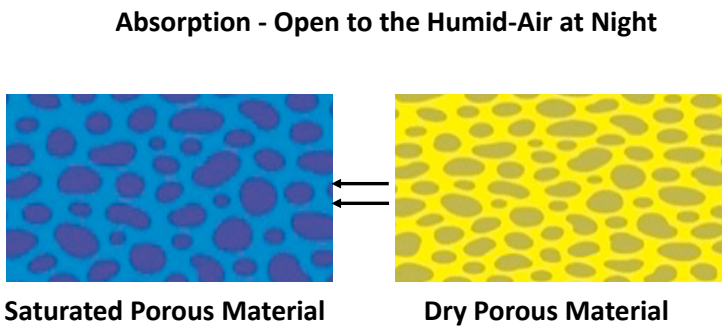

Figure 3. Schematic diagram of a harvesting atmospheric water system.

1.2. Research Motivation and Objectives

Although significant efforts have been made in the research of harvesting water from the atmosphere, to the best of the author's knowledge, no mathematical model has been conducted to specifically describe the process of harvesting water from the atmosphere using porous materials. The present study aims at developing a mathematical model and a reliable simulator describing the water moisture and analyzing HAW using porous materials. The study includes identifying porous materials in HAW, developing empirical formulas for a set of porous materials, and performing simulations by solving the set of governing partial differential equations numerically. Comparisons are presented to ensure the validity of the developed model. Several scenarios have been simulated and discussed with sensitivity analysis for the most important physical parameters.

1.3. Paper Outline

This paper is organized as follows: Section 2 provides an overview of the previous investigations of atmospheric water harvesting. Section 3 introduces the mathematical modeling developed in this study, including governing equations, associated parameterizations, and initial/boundary conditions. Section 4 presents the collected porous materials, and Section 5 has the proposed relative humidity-water content empirical model. Section 6 presents the results and discussion of the simulation. Finally, Section 7 draws the main conclusion and the most important findings while suggesting the key takeaways from the present study.

2. Literature Review

In the last few years, research efforts have been made to explore opportunities for freshwater sources. Water decontamination technologies such as filtration are employed to make wastewater safe. However, such technologies are possible in coastal regions, not landlocked areas, since they depend on natural water sources. Sultan et al. [22] studied two methods of extracting atmospheric water harvesting. Among the two was moisture adsorption through porous materials from atmospheric air. The authors compared the two methods, which included vapor compression and adsorption. It is found that HAW through adsorption is cheaper, ecologically friendly, and requires low thermal energy [23,24]. In the study by Adeyanju [25], a device for atmospheric harvesting water was developed. The device extracted water molecules and changed the phase to liquid from vapor. Moreover, the process involved air concentration through a porous, particularly solid. The porous is heated, thus allowing condensation, and the condensate is collected. Therefore, the study focus was on determining the relationship between nanoparticles of silica gel used and water produced to know the sufficient quantity needed for a given application. The result for the relationship was 1.0776 to 0.4752 with 10.7% efficiency. It involves experimentation, and results are obtained firsthand. The researchers tested the system in distinct conditions, thus proving its efficiency. Additionally, the device showed the possibility of atmospheric water extraction. Sleiti et al. [9] provided the designing, building, and testing of a device used in HAW. The device extracts water from the air with the help of adsorption materials.

The device's prototype consisted of silica gel. The researchers employed the prototype to conduct experimental studies in an indoor environment. Under various test conditions, including 22 degrees Celsius temperature, 60% RH, different silica thickness, and based on daily measurements, the harvester produced 800 mL for a 25 mm thickness. The study suggested various improvements for the HAW system, such as adding sorbent's multiple layers by employing enhanced adsorption properties. Sibie et al. [26] compared the water absorption abilities of different anhydrous salts such as magnesium sulfate, copper chloride, and copper sulfate. The mathematical model was used in water absorption simulation. Moreover, a comparison was made on results from distinct RH. For instance, under 15% RH, saturation rates registered in copper chloride, magnesium sulfate, and copper sulfate were 88.748, 76.825, and 81.797, respectively, which was in a static RH mode. The order was similar in dynamic RH mode. Moreover, the study has presented how the salts' sheet thickness, porous structure, and uniformity affected their absorption rate, which is significant for individuals who may need to develop a HAW device. Jarimi et al. [4] reviewed and described the performance of various atmospheric water collection technologies. The authors concluded that harvesting water from the atmosphere is available even in the driest climates, while fog can only occur in a limited number of areas, which reduces the contribution of fog harvesting techniques. Li et al. [27] studied 14 hydrated and anhydrous salt couples regarding their water harvesting and release capacities and thermal and chemical stabilities when applied in different scenarios. The salts screened in this laboratory experiment included magnesium sulfate, copper sulfate, copper chloride, nickel II nitrate, and iron II sulfate, among others. The first three salts ($MgSO_4$, $CuSO_4$, and $CuCl_2$) distinguished themselves and were used as water collection devices bilayers. The top layer was photothermal, while the bottom layer was a salt-fibrous membrane. It was found that these devices could capture water from the air even at a lower relative humidity of 15% and release the captured water at weakened sunlight of 0.7 kW/m^2. The researcher concluded that these anhydrous salts could produce clean water in areas where water is scarce. Wang et al. [10] investigated the water-adsorption capacity of birnessite, also known as the layered nanostructure MnO_2. They created the 800 nm or smaller diameter manganese oxide nanoparticles. The manganese oxide, MnO_2-1, has the best ability to adsorb water within a wide relative humidity range. The researchers conducted a water sorption test using the gravimetric vapor sorption instrument. From the result, it was found that water sorption of birnessite follows a type II isotherm. At the interlayers with low relative humidity, water molecules quickly adsorb. However, multi-layer water interactions happen through hydrogen bonding and condensed water at higher relative humidity. Birnessite was also found to have perfect solar absorptivity. They can be raised to 87 degrees Celsius with solar irradiation at a solar flux of approximately 900 W/m^2 to provide energy sufficient to trigger the desorption of interlayer water. With a dew point temperature of 111 degrees Celsius and relative humidity of 23%, birnessite can harvest 0.07 kg of water per kilogram sample. The researcher built a device to present the application based on their experiment. The study concluded that adsorption material with higher solar absorptivity, such as birnessite, is appropriate for producing clean water in areas where water is scarce. Gordeeva et al. [28] studied the water sorption equilibrium of lithium bromide nanoparticles confined to microporous expanded graphite and mesoporous synthetic carbon subunit pores. The researchers found that the two composites exhibited different water sorption equilibrium with the isobars of expanded graphite samples, forming a plateau corresponding to one molecule of water adsorbed on one molecule of lithium bromide (LiBr) nanoparticles. Thus, the host porous material is filled with a nanofluid made of lithium bromide LiBr nanoparticles ranging in size from 500 to 900 nm. This indicated the crystallization of a hydrate ($LiBr.H_2O$) inside the ports of the expanded graphite, a monovariant equilibrium. It was also found that lowering the temperatures could make this equilibrium divariant, which is typical with LiBr water solutions. On the other hand, no water was formed in the pores of the mesoporous synthetic carbon subunit as the equilibrium remained divariant at all temperature ranges. The differences were associated with the structural difference of

the host carbon pores. For this reason, sorbents can be used in drying gas, thermal energy storage, and many other applications.

On the other hand, the desiccant's chemical and physical characteristics facilitate greater water absorption. Zhang et al. [29] used porous silica gel as a host for $CaCl_2$; however, the equilibrium process took 35 h as opposed to 4 h when carbon nanotubes were used. Temperature and relative humidity are two carrying capacity parameters that impact the processing pace. Surface area, wind speed, and liquid desiccant flow, on the other hand, affect how quickly or slowly the sorbent will achieve equilibrium. For instance, it was observed that a composite of 85% $CaCl_2$ and 15% LiBr could absorb three times as much as $CaCl_2$ alone could [30]. Elashmawy et al. [31] collected 1.06 $L/m^2/day$ utilizing five shelves to enhance the surface area on a black cotton cloth as the host for their studies. Recently, Almasarani et al. [32] conducted several experiments to predict and improve water absorption and desorption behavior by the calcium chloride desiccant. They investigated the absorption effect in a deep container, which intensified by adding air to the mixture. The latter assessed how much water a thin solution layer absorbed or lost when exposed to various environmental factors. When applying a thin solution coating, air pumping inside deep liquid desiccant containers boosted the water absorption rate to 3.75% per hour.

Based on findings from the above literature review, using porous materials in HAW is the preferred means of water extraction from the atmosphere for various reasons. For instance, the designs require little energy, are environmentally friendly, and are cheap. The studies also make the systems more competitive than the existing ones, including water distillation. Studies suggest that enhanced and efficient units are designed through experience from porous cooling studies. Moreover, the studies also indicate that HAW is eased by adapting fiscal investment and employing safer energy sources, which are more likely to be porous materials. The shared key target in all previous literature reviews is to develop different experimental techniques to reduce water shortages. However, to the best of the authors' knowledge, neither mathematical modeling nor numerical simulation has been devoted to analyzing atmospheric water harvesting using porous materials.

3. Mathematical Modeling

This section details the development of the mathematical model describing the water moisture and analyzing atmospheric harvesting water using porous materials. The governing partial differential equations, including conservation mass equation, momentum equation (Darcy's law), associated parameterizations, and initial/boundary conditions, were developed to represent water moisture absorption using porous materials.

In volumetric moisture content, the amount of moisture in a porous media, i.e., water in the liquid and/or vapor phase, is stated. The mass conservation equation describes the total moisture balance in porous media since water occurs in both liquid and gaseous phases [33]; the equation is given by

$$\frac{\partial}{\partial t}(\rho_L\theta + \rho_V\theta_a) = -\frac{\partial}{\partial z}q_m \tag{1}$$

where $\rho_L\left(\mathrm{kg\ m^{-3}}\right)$ is the density of the liquid water, $\rho_V\left(\mathrm{kg\ m^{-3}}\right)$ is the density of water vapor, θ the volumetric water content, θ_a the gas phase volumetric air content, z is the vertical space coordinate positive upwards, and finally, $q_m\left(\mathrm{kg\ m^{-2}s^{-1}}\right)$ represents the porous moisture flux in both vapor and liquid phases. The water vapor and formed water liquid flow in the porous material can be described by the contribution of two terms, Fick's first law of diffusion and Darcy's law, and given by [34]

$$q_m = q_L + q_V = -\rho_L k_H \frac{\partial h}{\partial z} - D_e \frac{\partial \rho_V}{\partial z} \tag{2}$$

where q_L represents liquid flux (kg $m^{-2}s^{-1}$), q_V represents vapor flux (kg $m^{-2}s^{-1}$), k_H represents hydraulic conductivity (m s^{-1}), h represents the hydraulic head (m), and D_e represents molecular diffusivity of water vapor (m^2s^{-1}). The first term on the equation's right-hand side (RHS) represents liquid flow (2). The final component of the equation represents the water vapor flow since water vapor density is a function of matric potential and temperature. Only the isothermal case was examined. A parameterization equation is added for the gas and liquid phases since the independent and dependent variables are related, as discussed in the following subsections. Note that all dependent variables must be calculated from the set of independent variables. For the liquid and gas phases, parameterization was added. Philip and De Vries [35] explained the link between relative humidity and hydraulic head:

$$H_r = \exp\left(\frac{hg}{R_v T}\right) \tag{3}$$

where R_v is the water vapor-specific gas constant 461.5 (J $kg^{-1}K^{-1}$), and g is the gravitational acceleration (m s^{-2}), and T is the temperature (K). The chain rule of Equation (3) produces

$$\frac{\partial h}{\partial z} = \frac{R_v T}{g H_r}\frac{\partial H_r}{\partial z} \tag{4}$$

The density of water vapor in the gas phase is estimated using Philip and De Vries' formula [35]

$$\rho_v = \rho_{sv} H_r \tag{5}$$

where H_r is the relative humidity, and ρ_{sv} (kg m^{-3}) is the density of saturated water vapor. The saturated vapor density is a temperature-dependent property that may be calculated using the method below [35].

$$\rho_{sv} = \frac{10^{-3}}{T}\exp\left(31.3716 - \frac{6014.79}{T} - 7.92495 \times 10^{-3}T\right) \tag{6}$$

The vertical gradient of water vapor density may be expressed as [35]

$$\frac{\partial \rho_V}{\partial z} = \rho_{sv}\frac{\partial H_r}{\partial z} \tag{7}$$

The porosity value, which varies from 0 to 1, is equal to the sum of the liquid and vapor content that saturate vacant space in a porous material:

$$\varepsilon = \theta_a + \theta \tag{8}$$

Milly [33] defined D_e as the water vapor diffusivity in porous materials

$$D_e = \theta_a D_a \tag{9}$$

D_a (m^2s^{-1}) is the water vapor diffusivity in the atmosphere at temperature T (K) [36]

$$D_a = 2.12 \times 10^{-5}\left(\frac{T}{273.15}\right)^2 \tag{10}$$

Finally, the atmospheric water harvesting model is created using Equations (2) through (10):

$$\frac{\partial}{\partial t}(\rho_L\theta + \rho_{sv}H_r(\varepsilon - \theta)) = \frac{\partial}{\partial z}\left(\left(\rho_L k_H \frac{R_v T}{g H_r} + (\varepsilon - \theta)D_a\rho_{sv}\right)\frac{\partial H_r}{\partial \theta}\frac{\partial \theta}{\partial z}\right) \tag{11}$$

This unclosed system needs to have a defined relative humidity function in terms of the water content, $H_r(\theta)$. This will be achieved by collecting data from the literature and forming the function $H_r(\theta)$, as shown below in Sections 4 and 5.

The water content meets the starting criteria of the form at time t = 0 for all z:

$$\theta(z, t = 0) = \theta_0 \tag{12}$$

The following boundary conditions are also required by solution components:

$$\theta(z = 0, t) = \theta_{tb} \tag{13}$$

It indicates the upper boundary's water content (Dirichlet boundary condition):

$$\frac{\partial\theta}{\partial z}(z = L, t) = 0 \tag{14}$$

This is a Neumann-type boundary condition that represents a no-flow boundary.

4. Porous Materials Used in HAW Model

This section describes materials with which their data were gathered during the literature review to build the HAW model.

4.1. Copper Chloride

Copper chloride is a chemical compound in both anhydrous and dihydrate forms. Its chemical formula is $CuCl_2$. When it is in anhydrous form, its color is yellowish-brown, and in dihydrate form, it is green. Copper chloride has an excellent capacity for absorbing and releasing water. It is also chemically and physically very stable. Copper chloride also has a high capacity for absorbing light [27].

4.2. Copper Sulfate

Copper sulfate is an inorganic compound and has a chemical formula of $CuSO_4$. It is in the form of blue crystals and can contain up to five molecules of water. The anhydrous form is obtained by heating the hydrous form. Copper sulfate has a suitable capability of storing or releasing water content. It is also chemically and physically very stable. However, $CuSO_4$ has a lower light-absorbing capacity [27].

4.3. Magnesium Sulfate

Magnesium sulfate is a color compound in the form of a crystal, and it has many applications in the medical field. Its chemical formula is $MgSO_4$. $MgSO_4$ is used in devices designed to collect water vapors or release water assisted by photothermal devices. In such cases, $MgSO_4$ is generally used in areas where the humidity is high, and there is less radiation from the sun. Magnesium sulfate has a suitable capability of storing or releasing water content and a very stable [27].

4.4. MnO_2-1

The manganese oxides are prepared by adding 1 g of potassium permanganate ($KMnO_4$) to about 75 mL of deionized water (H_2O) and dissolving in it. To prepare the oxides, varying quantities of manganese (II) salt ($MnSO_4H_2O$) are added. To prepare MnO_2-1, 0.1 g of manganese (II) salt ($MnSO_4H_2O$) is added to the above solution. Manganese dioxide (MnO_2) is found largely in nature. It consists of both tunnel and layered structures. The structure of MnO_2-1 consists of nanoflower spheres stacked with a sheet. The diameter of these spheres ranges from ~800 nm. For a wide range of relative humidity, MnO_2-1 has the best capability of adsorbing water [10].

4.5. SWS-2EG

SWS stands for selective water sorbents. It refers to a new material developed to produce freshwater from the atmosphere. This material consists of a system of two phases. One is a host matrix that consists of pores, and the other is a hygroscopic substance. This substance is infused into the pores of the host matrix. SWS-2EG is a sorbent that consists of crystallites of lithium bromide (LiBr). The size of these crystallites varies from 500 to 900 nm. It possesses a high capability of water sorption. It also has a high energy storage capacity, which makes it useful in the applications of storage of thermal energy [28].

5. Relative Humidity Model

The relationship between the RH and water content has been used based on Philip and De Vries [35]

$$H_r = \frac{P}{P_0} = \exp\left(-\frac{g\,\psi(\theta)}{R_v T}\right) \tag{15}$$

where g is gravity (m/s^2), T is the temperature (K), R is the ideal gas constant, and $\psi(m)$ is suction, which is a function of real volumetric liquid moisture content $\theta(m^3/m^3)$ and represents the capillary forces of a porous material's whole network.

To create a relationship between the relative humidity and the water content, $\psi(\theta)$ the model was developed by collecting the data from Li et al. [27], Wang et al. [10], and Gordeeva et al. [28], who investigated five different porous materials for atmospheric harvesting water, and by using the negative power best-fit method for each material as shown in Figures 3–7, $\psi(\theta)$ is derived:

$$\psi(\theta) = \alpha\theta^{-\beta} \tag{16}$$

where α, β are constants, and Table 1 below shows the values of α and β for each material. In addition, the fourth and fifth column of Table 1 shows the R-squared correlation of the two functions $\psi(\theta)$ and $H_r(\theta)$, respectively. From this table, it can be seen that the correlation coefficient of the relative humidity functions is much better than it for the function $\psi(\theta)$. In general, the models of copper chloride and magnesium oxide were the best as they have the highest correlation coefficient values. Although the error in Figures 5 and 6 looks a bit high, however, it does not significantly affect the absorbed water content, as will be discussed below in the Results and Discussion section.

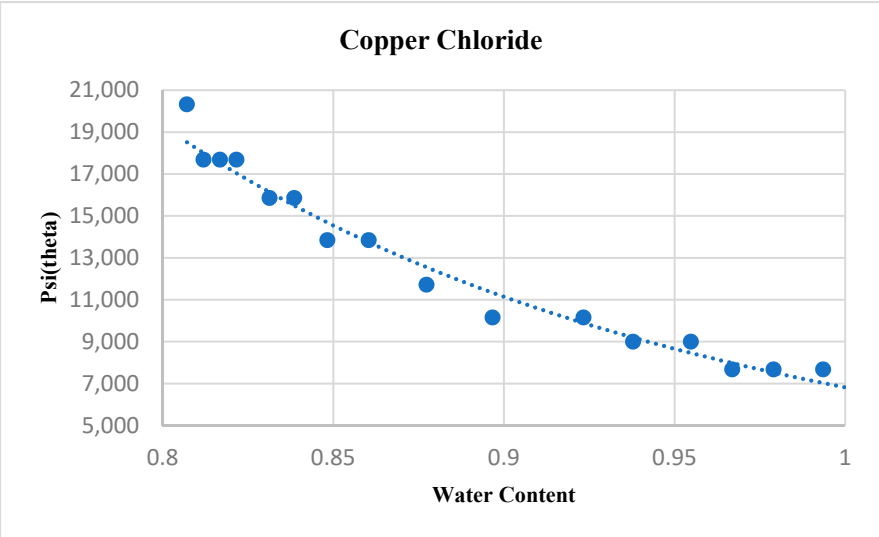

Figure 4. Decay model for copper chloride.

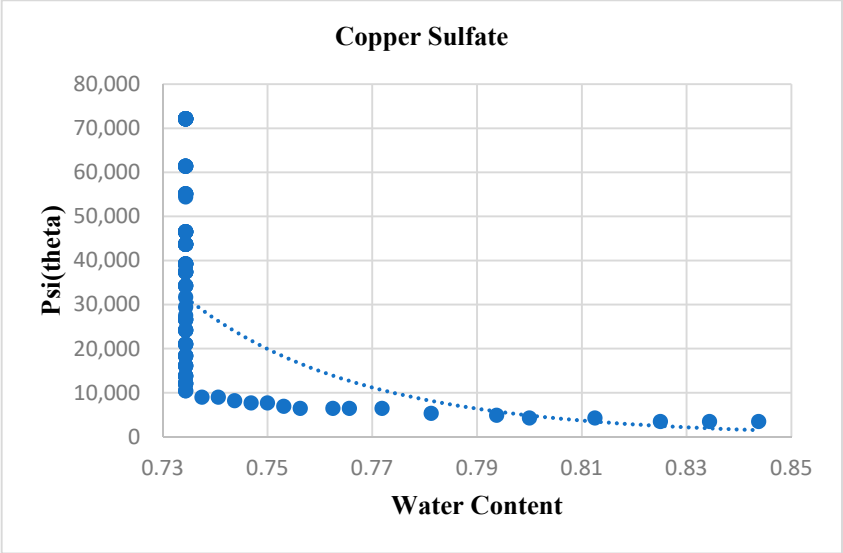

Figure 5. Decay model for copper sulfate.

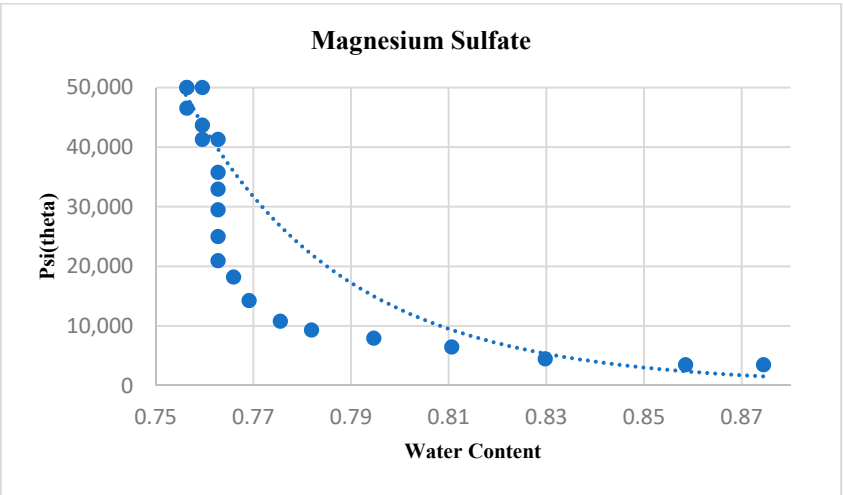

Figure 6. Decay model for magnesium sulfate.

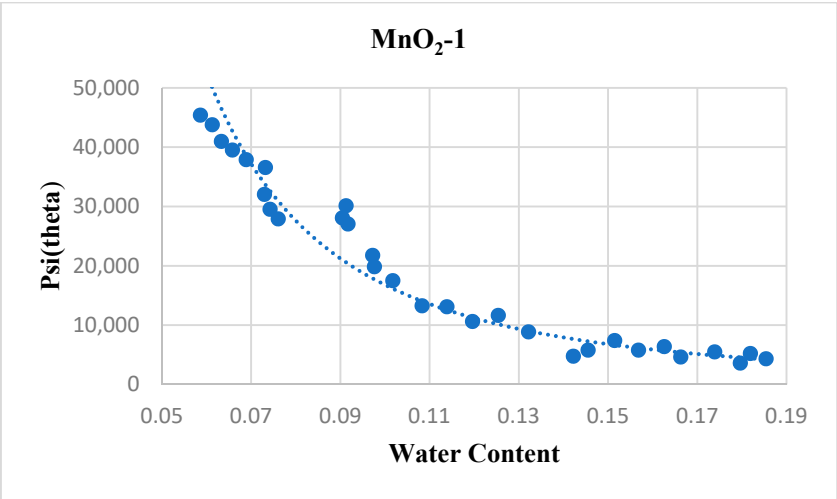

Figure 7. Decay model for MnO_2-1 nanoparticles.

Table 1. Estimation of α and β for each material.

Porous Materials	α	β	R^2, ψ(θ)	R^2, $H_r(\theta)$
Copper Chloride	6821	4.661	0.98780	0.98926
Copper Sulfate	36.635	21.9	0.52737	0.73621
Magnesium Sulfate	63.849	23.75	0.86528	0.90572
MnO_2-1	79.219	2.338	0.91026	0.95684
SWS-2EG	26051	0.388	0.75640	0.92507

This section compares the simulated relative humidity model and the experimental relative humidity model. The data from three SWS-2EGs were utilized to create the comparison [27]. It is predicted that the water content of various SWSs would rise with increasing relative humidity. The three SWS-2EG were subjected to different relative humidity values at a constant temperature.

SWS-2EG shows the water sorption equilibrium, which qualitatively differs for the two hosts: the expanded graphite and carbon subunit. It indicated the formation of a hydrate LiBr-H_2O nanofluid inside the expanded graphite ports, a monovariant equilibrium. Lowering the temperatures were also discovered to make this equilibrium variant typical of LiBr nanoparticle water solutions. However, no water was formed in the pores of the mesoporous synthetic carbon subunit because the equilibrium remained variant across all temperature ranges [28].

Figure 8 illustrates that water content for SWS-2EG increases with relative humidity. However, the relationship is also exponential. Overall, the water-holding capacity for SWS-2EG nanoparticles does not change at a constant rate with relative humidity. The results also indicate that the water content capacity increases up to a certain point for relative humidity. After this value, the water capacity of the materials might start to decrease or remain constant. Hence, the materials might be efficient in regions with optimal relative humidity.

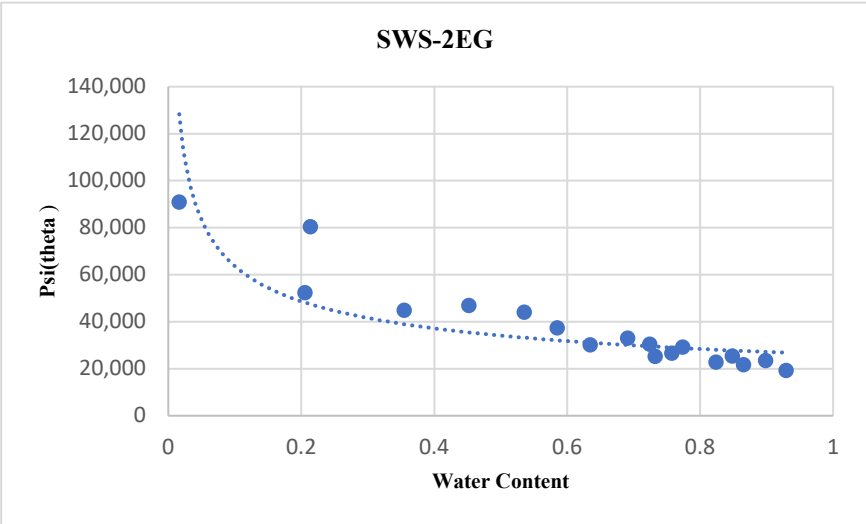

Figure 8. Decay model for SWS-2EG.

6. Results and Discussion

The above highly nonlinear partial differential equation is solved numerically using an efficient algorithm. The governing Equations (1)–(11) are solved along with their initial and boundary conditions Equations (12)–(14). The Galerkin method handles spatial discretization, while an adaptive time step is used with the time integration. The mathematical equations, along with initial and boundary conditions developed in the previous sections, are solved numerically using the MATLAB function "pdepe" (parabolic and elliptic) [37]. MATLAB is one of the high-level programming languages that contains efficient

libraries with high accuracy. Therefore, we selected to write our code using MATLAB programming language.

The number of spatial discretizations ranged from 200 to 600 cells depending on the depth of the sample. The time step of this algorithm is adaptable based on the error tolerance. The 'pdepe' function uses 'odeset' options-defined integration parameters. For instance, the options "AbsTol" and "RelTol" can be assigned to define the desired absolute and relative error tolerance, respectively. Therefore, in this study, we selected a relative error tolerance of 10^{-6} using the following statement: "options = odeset ('RelTol',1e-6)".

The moisture absorption for the materials: copper chloride ($CuCl_2$), copper sulfate ($CuSO_4$), magnesium sulfate ($MgSO_4$), MnO_2-1 nanoparticles, and SWS-2EG nanoparticles are considered. The physical parameters used in the model have been presented in Table 2. The parameters used in the model have been presented in Table 3. The initial condition of the water content of copper chloride is taken as θ_0 =0.79 (79%), and the boundary condition is taken as θ_{tb} =0.99 (99%). The depth varies from 0 to 0.04 m. The time varies from 0 min to 1000 min. The initial condition of the water content of copper sulfate is also taken as θ_0 =0.73 (73%), and the boundary condition is taken as θ_{tb} =0.85 (85%). The depth varies from 0 to 0.15 m. The time varies from 0 min to 1000 min. Furthermore, the initial condition of the water content of magnesium sulfate is taken as θ_0 =0.68 (68%), and the boundary condition is taken as θ_{tb} =0.87 (87%). The total depth is 0.16 m. The time varies from 0 min to 1000 min. In addition, the initial condition of the water content of MnO_2-1 is taken as θ_0 =0.053 (5.3%), and the boundary condition is taken as θ_{tb} =0.193 (19.3%). The total depth is 0.08 m. The time varies from 0 min to 300 min. Further, the initial condition of the water content of SWS-2EG is taken as θ_0 =0.016 (1.6%), and the boundary condition is θ_{tb} =0.93 (93%). The total depth is 0.08 m. The time varies from 0 min to 1500 min.

Table 2. Physical parameters.

Name	Symbol	Value	Unit
Density of water	ρ_L	997	$\left[kgm^{-3}\right]$
Temperature	T	320	[K]
Specific gas constant for water vapor	R_v	461.5	$J\ kg^{-1}K^{-1}$

Table 3. Materials parameters.

	Depth (m)	Time (min)	$k_H \times 10^{-10}$	ε	θ_{tb}	θ_0
Copper Chloride	0.04	1000	5.5556	0.37	0.99	0.79
Copper Sulfate	0.15	1000	3.7256	0.33	0.85	0.73
Magnesium Sulfate	0.16	1000	0.1160	0.41	0.87	0.68
MnO_2-1	0.08	300	9.8301	0.48	0.193	0.053
SWS-2EG	0.08	1500	1.0316	0.42	0.93	0.016

The validity and robustness of the suggested model may be shown by the fact that experimental and simulation findings are in close agreement. Figure 9 compares the simulated relative humidity model and the experimental one. The data from SWS-2EG [28] were utilized to create the comparison. It indicates that the water absorption capacity of SWS-2EG increases with increasing relative humidity.

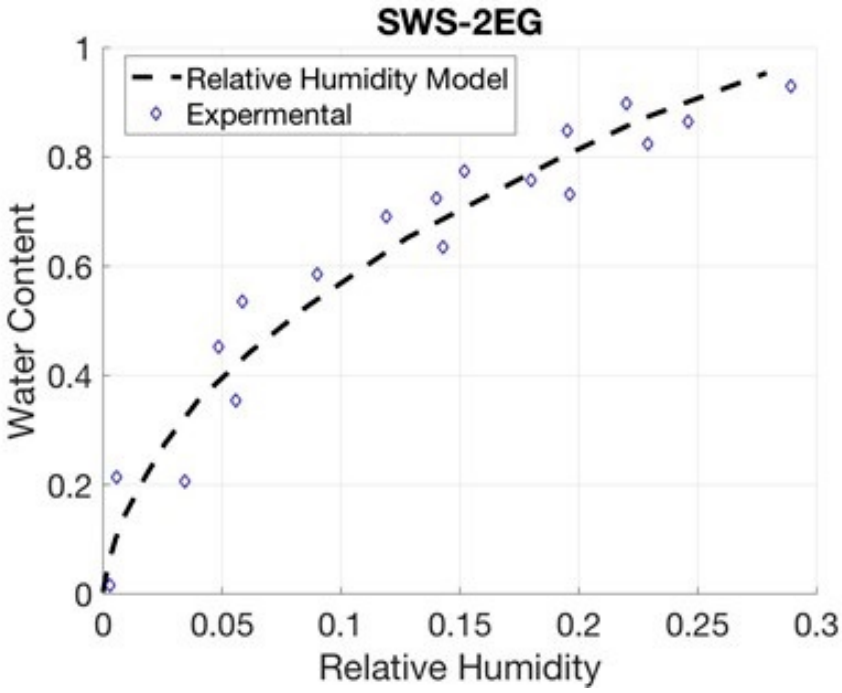

Figure 9. Comparison of relative humidity model of SWS-2EG nanoparticles [28].

Figures 10–13 show a comparison between the experimental and simulated absorption of the water content of porous materials from the atmosphere with time. The experimental data are taken from the references [10,27]. As time increases, the absorption of water will increase. The simulated results are very close to the experimental results. The comparison in Figure 10 shows a few variations. Initially, the absorption of water of copper chloride from the atmosphere is less in experimental results than in simulated results.

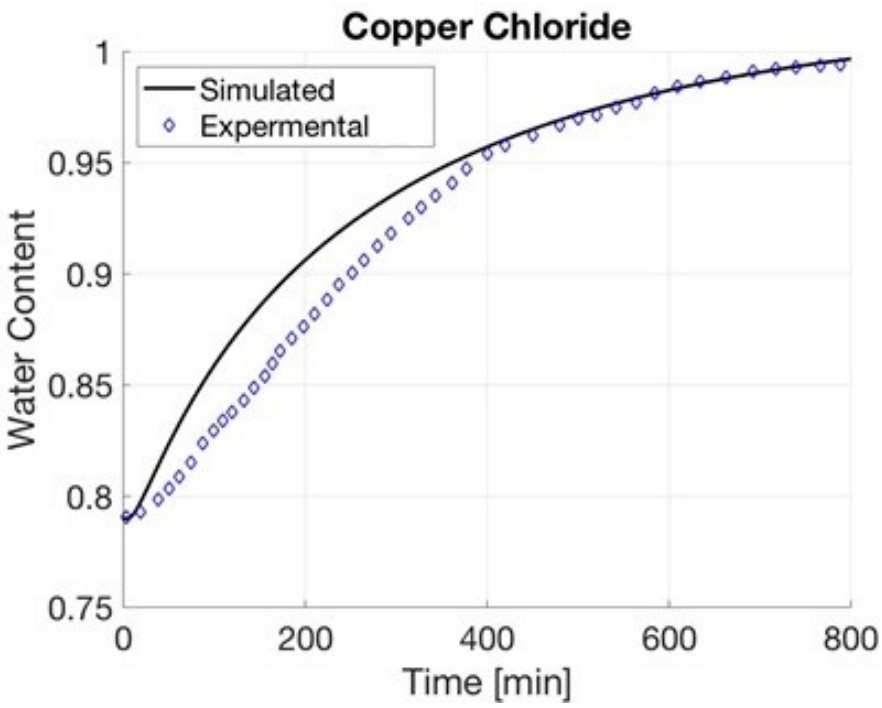

Figure 10. Comparison of HAW model of copper chloride [27].

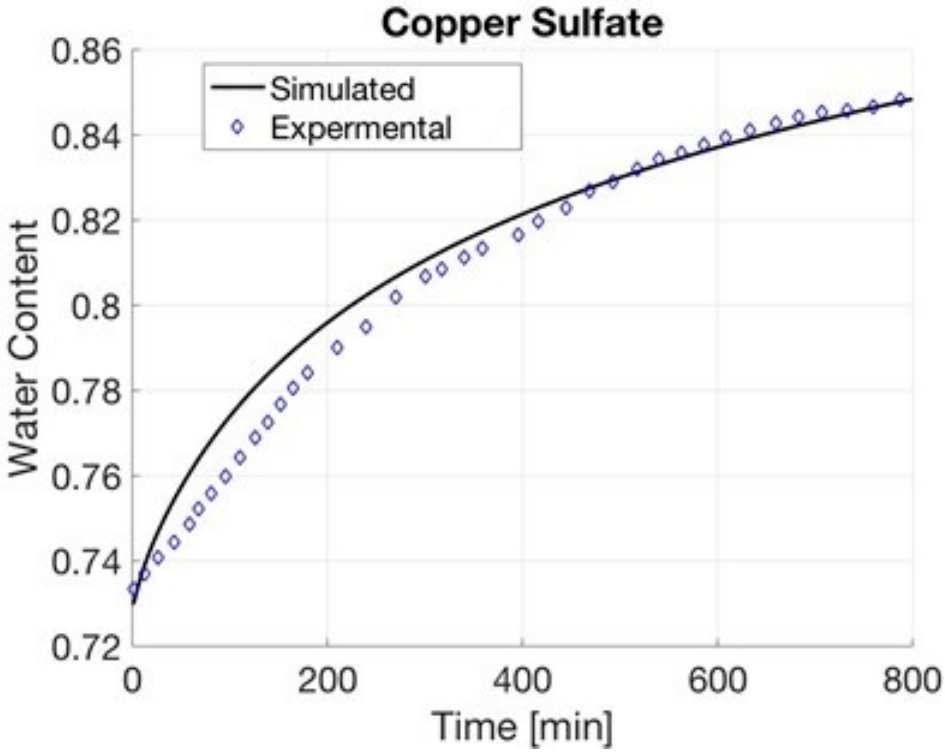

Figure 11. Comparison of HAW model of copper sulfate [27].

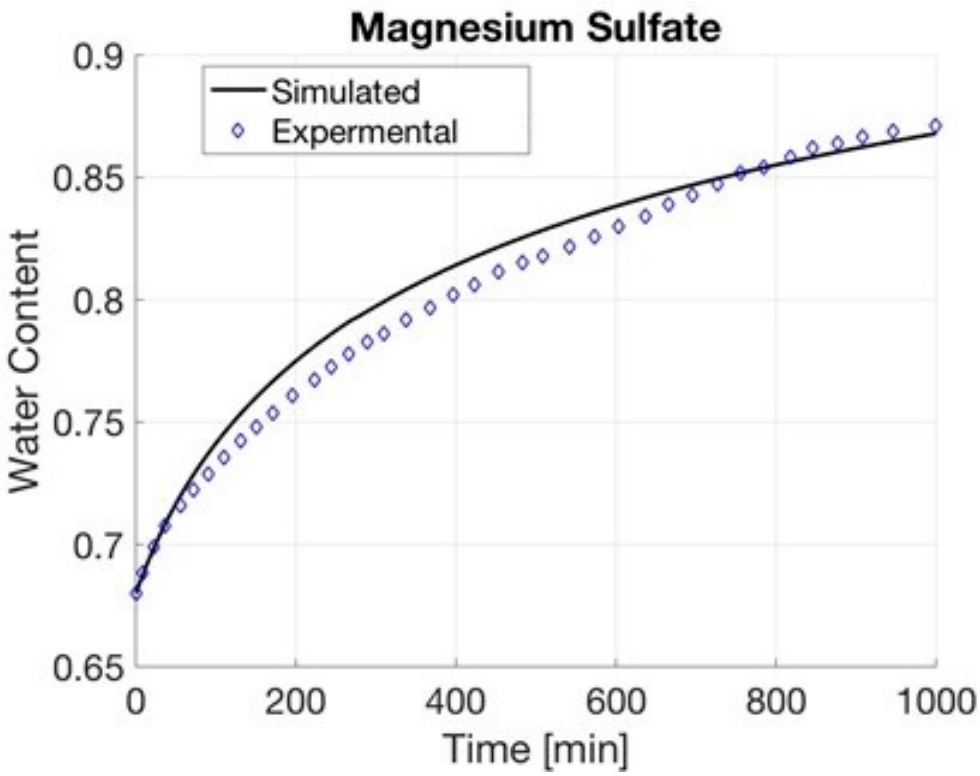

Figure 12. Comparison of HAW model of magnesium sulfate [27].

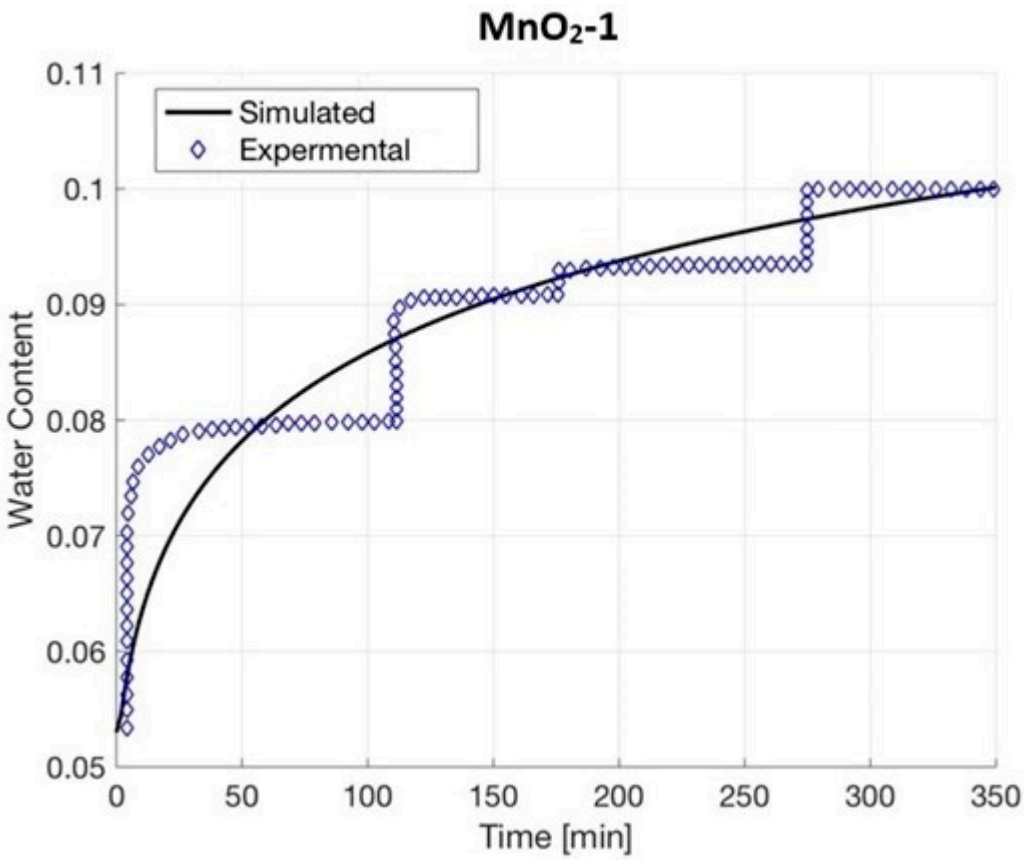

Figure 13. Comparison of HAW model of MnO_2-1 (a) [10].

At the beginning (0 min to approximately 400 min), a few differences may be seen in the comparison in Figure 11. When simulated findings are compared to experimental data, the absorption of water of copper sulfate from the atmosphere is shown to be smaller in the simulated results. Still, it is better than the copper chloride comparison.

The comparison of simulated magnesium sulfate results with experimental findings is shown in Figure 12. The findings were the same at the start and the conclusion, with just a minor difference appearing in the middle, between around 100 min and 800 min of absorbing time.

Here, the experimentation includes water vapor adsorption by MnO_2. The considered experiment has been segregated into five segments, in which water content, time, and MnO_2's capacity to absorb water have been considered the prime variables. The first phase has been experimented with two times, considering the change in the water content absorption capacity of two types of MnO_2 and the timing. In the first case, the extraction of water molecules from the atmosphere includes a zigzag shape, and the increment in water content rises from 5% to 10% during 350 min (Figure 13). Whereas the second experiment of the first phase showcases the presence of a higher degree of water vapor within the atmosphere, the characteristics of MnO_2-1 resulted in reaching the water content range of 14%–19.4% of water content and gradually increased over 30 min (Figure 14). In this experiment segment, the simulation and actual result follow a similar pathway of increment in water absorption.

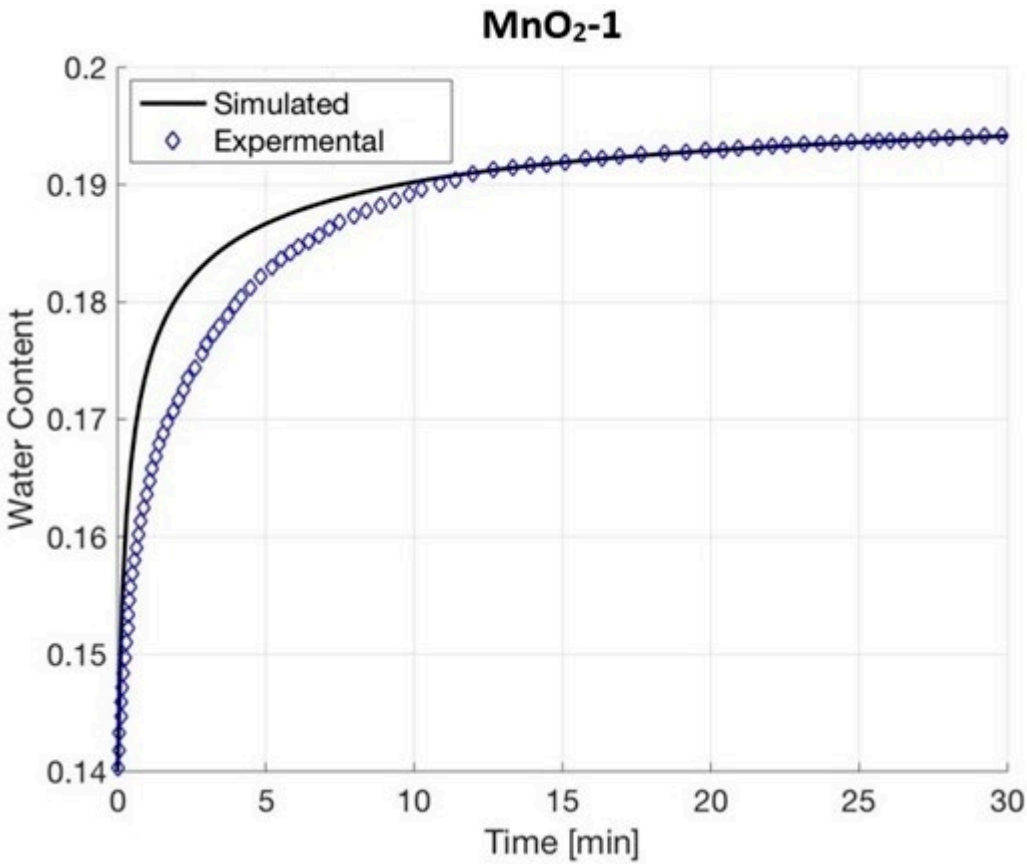

Figure 14. Comparison of HAW model of MnO_2-1 (b) [10].

The relative error of the proposed model was determined to demonstrate its validity and robustness. Table 4 shows the maximum and minimum errors and the average for all the relative error points. The maximum error of the harvesting atmospheric water model of copper chloride is around 1.29%, the minimum error is about 0.025%, and the average error of the HAW model of copper chloride is 0.49%. Furthermore, the maximum error of the HAW model of copper sulfate is around 0.77%, the minimum error is about 0.01%, and the average error of the HAW model of copper sulfate is 0.31%. In addition, the maximum error of the HAW model of magnesium sulfate is around 1.4%, the minimum error is about 0.001%, and the average error of the HAW model of magnesium sulfate is 0.66%. Further, the maximum error of the HAW model of MnO2-1 is around 7.72%, the minimum error is about 0.001%, and the average error of the HAW model of MnO_2-1 is 1.88%.

$$\text{Relative error } \% = \frac{|\text{ Simulation} - \text{ Experimental}|}{\text{Experimental}} \times 100 \tag{17}$$

Table 4. Relative error for porous materials.

Porous Materials	Maximum Error %	Minimum Error %	Average for All the Relative Error Points %
Copper Chloride	1.28605756%	0.0251514%	0.49353302%
Copper Sulfate	0.76765625%	0.01021925%	0.31534476%
Magnesium Sulfate	1.33724095%	0.0013657%	0.6653724%
MnO_2-1	7.72054771%	0.00105762%	1.87852984%

The moisture absorption rate by specific porous materials depends on various factors such as temperatures, relative humidity, thickness, and time. It is not easy to estimate the

absorption of moisture rate. However, it is easy to determine the highest quantity of water that could be absorbed under given conditions. Consequently, this section displays the simulated water content for each material and the amount of time in minutes, along with the depth in meters (m) for each material and a three-dimensional surface that plots to map three variables: water content (θ), depth (m), and time (min).

In Figure 15, there are five gradients for five different porous materials. The first curve with the dark blue color shown explains copper chloride. The second curve with the red color shown describes copper sulfate. The third curve with the black shown defines magnesium sulfate. The curve with the light blue shown describes SWS-2EG. The last curve with the light green color shows MnO_2-1. It shows that SWS-2EG has a low initial value but lies above all other materials. Variants of MnO_2-1 show the lowest water content in a similar span. However, copper chloride has a percentage change of around 25.31%. On the other hand, copper sulfate has a percentage change of approximately 16.44%, the lowest percentage change. Furthermore, magnesium sulfate has a percentage change of around 27.94%.

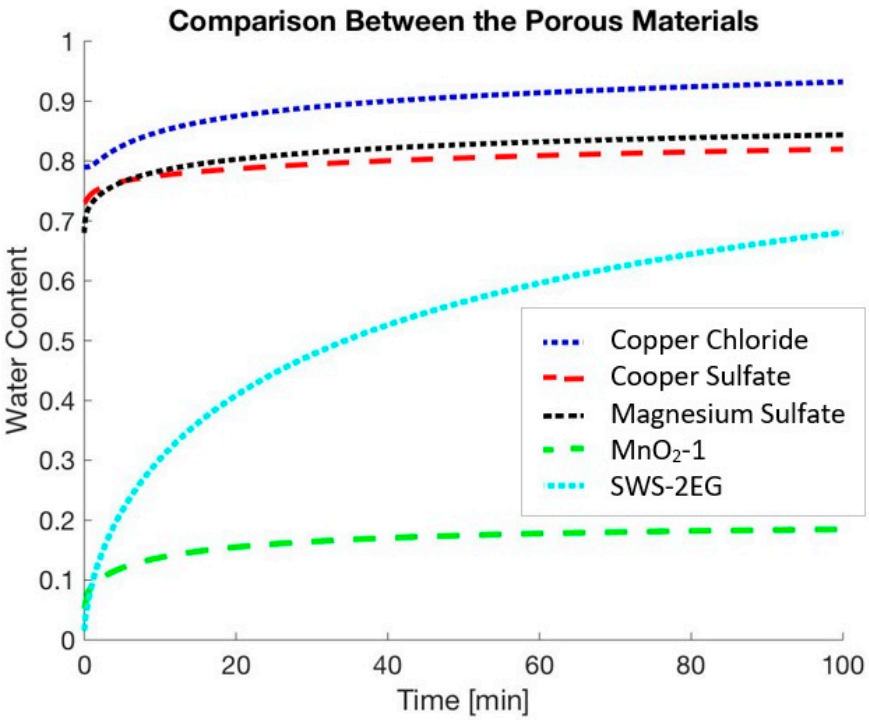

Figure 15. Comparison between the water content from different porous materials.

7. Conclusions

Harvesting water from the atmosphere is becoming the most viable option for supplying freshwater as water is abundant in the atmosphere. Porous materials in HAW are the preferred means of water extraction from the atmosphere. The designs require little energy, are environmentally friendly, and are cheap. However, the efficiency of an atmospheric water harvesting system depends on relative humidity, temperature, water sorption capacity based on the adsorption phenomenon, and other factors. This paper mainly developed a reliable mathematical model for water moisture absorption by porous materials to simulate and analyze HAW harvesting. A group of governing partial differential equations, including the conservation mass equation, momentum equation, associated parameterizations, and initial/boundary conditions, make up the mathematical model. The model includes phase-change gas–liquid physics, which simulates a two-phase fluid flow. Different times, thicknesses, and other crucial characteristics were considered in the simulated model. A dataset compiled from the literature containing five porous materials has been tested in producing water from the air. A series of empirical models to relate relative humidity and

water content have been proposed and combined with the governing to close the mathematical system. A comparison with experimental results demonstrated the simulation model's validity. The findings revealed that the mathematical model proposed accurately predicts water content during the absorption process. Furthermore, the simulation findings showed that when the depth is smaller during the absorption process, the water content reaches a greater saturation point fast, i.e., quick process. Finally, the HAW model's highest average error is roughly 1.9% compared to experimental data observed in MnO_2-1. As a result, the HAW model is appropriate.

Author Contributions: Conceptualization, M.F.E.-A.; Data curation, S.S.A.; Formal analysis, M.F.E.-A.; Investigation, M.F.E.-A. and S.S.A.; Methodology, M.F.E.-A.; Resources, T.B.; Validation, M.F.E.-A. and S.S.A.; Writing—original draft, S.S.A., M.F.E.-A. and T.B.; Writing—review and editing, M.F.E.-A. All authors have read and agreed to the published version of the manuscript.

Funding: The authors gratefully acknowledge the support of DGSR at Effat University, Jeddah, Saudi Arabia, for Internal Grant No. UC#9/1June2022/7.1-21(4)3, Code: S2022-14-3.

Data Availability Statement: Data are available in the manuscript.

Conflicts of Interest: The authors declare that they do not have any conflict of interest.

References

1. UNESCO. The United Nations World Water Development Report 2021: Valuing Water. UNESCO: Paris, France, 2021. Available online: https://unesdoc.unesco.org/ark:/48223/pf0000375724 (accessed on 14 June 2022).
2. Gleick, P.H. (Ed.) *Water in Crisis: A Guide to the World's Fresh Water Resources*, Illustrated ed.; Oxford University Press: New York, NY, USA, 1993.
3. UNICEF. Billions of People Will Lack Access to Safe Water, Sanitation and Hygiene in 2030 unless Progress Quadruples–Warn WHO, UNICEF. UNICEF for Every Child. 1 July 2021. Available online: https://www.unicef.org/press-releases/billions-people-will-lack-access-safe-water-sanitation-and-hygiene-2030-unless (accessed on 30 November 2021).
4. Jarimi, H.; Powell, R.; Riffat, S. Review of sustainable methods for atmospheric water harvesting. *Int. J. Low-Carbon Technol.* **2020**, *15*, 253–276. [CrossRef]
5. Tu, Y.; Wang, R.; Zhang, Y.; Wang, J. Progress and Expectation of Atmospheric Water Harvesting. *Joule* **2018**, *2*, 1452–1475. [CrossRef]
6. Cherif, H.; Belhadj, J. Chapter 15-Environmental Life Cycle Analysis of Water Desalination Processes. In *Sustainable Desalination Handbook*; Gude, V.G., Ed.; Butterworth-Heinemann: Oxford, UK, 2018; pp. 527–559. [CrossRef]
7. Curto, D.; Franzitta, V.; Guercio, A. A Review of the Water Desalination Technologies. *Appl. Sci.* **2021**, *11*, 670. [CrossRef]
8. Dhakal, N.; Salinas-Rodriguez, S.G.; Hamdani, J.; Abushaban, A.; Sawalha, H.; Schippers, J.C.; Kennedy, M.D. Is Desalination a Solution to Freshwater Scarcity in Developing Countries? *Membranes* **2022**, *12*, 381. [CrossRef]
9. Sleiti, A.K.; Al-Khawaja, H.; Al-Khawaja, H.; Al-Ali, M. Harvesting water from air using adsorption material—Prototype and experimental results. *Sep. Purif. Technol.* **2020**, *257*, 117921. [CrossRef]
10. Wang, J.; Dang, Y.; Meguerdichian, A.G.; Dissanayake, S.; Kankanam-Kapuge, T.; Bamonte, S.; Tobin, Z.M.; Achola, L.A.; Suib, S.L. Water Harvesting from the Atmosphere in Arid Areas with Manganese Dioxide. *Environ. Sci. Technol. Lett.* **2019**, *7*, 48–53. [CrossRef]
11. Fernandez, D.M.; Torregrosa, A.; Weiss-Penzias, P.S.; Zhang, B.J.; Sorensen, D.; Cohen, R.E.; McKinley, G.H.; Kleingartner, J.; Oliphant, A.; Bowman, M. Fog Water Collection Effectiveness: Mesh Intercomparisons. *Aerosol Air Qual. Res.* **2018**, *18*, 270–283. [CrossRef]
12. Cruzat, D.; Jerez-Hanckes, C. Electrostatic fog water collection. *J. Electrost.* **2018**, *96*, 128–133. [CrossRef]
13. GENAQ. Atmospheric Water Generator by GENAQ. A New Water Supply Alternative. Available online: http://www.genaq.com/water/ (accessed on 28 November 2021).
14. Shourideh, A.H.; Ajram, W.B.; Al Lami, J.; Haggag, S.; Mansouri, A. A comprehensive study of an atmospheric water generator using Peltier effect. *Therm. Sci. Eng. Prog.* **2018**, *6*, 14–26. [CrossRef]
15. Precipitation Formation from Orographic Cloud Seeding. PNAS. Available online: https://www.pnas.org/content/115/6/1168 (accessed on 20 September 2021).
16. World Economic Forum. Unusual Methods to Harvest Earth's Untapped Water Sources. Available online: https://www.weforum.org/agenda/2021/02/water-scarcity-shortage-sustainability-climate-change-innovation-resources/ (accessed on 20 September 2021).
17. Gado, M.G.; Nasser, M.; Hassan, A.A.; Hassan, H. Adsorption-based atmospheric water harvesting powered by solar energy: Comprehensive review on desiccant materials and systems. *Process Saf. Environ. Prot.* **2022**, *160*, 166–183. [CrossRef]
18. Qi, S.; Zhuang, H.; Wang, X.; Li, X.; Liu, K.; Liu, J.; Zhang, H. Advances in solar-driven hygroscopic water harvesting. *Glob. Chall.* **2021**, *5*, 2000085.

19. Asim, N.; Badiei, M.; Alghoul, M.A.; Mohammad, M.; Samsudin, N.A.; Amin, N.; Sopian, N.K. Sorbent-based air water-harvesting systems: Progress, limitation, and consideration. *Rev. Environ. Sci. Bio/Technol.* **2021**, *20*, 257–279. [CrossRef]
20. Bilal, M.; Sultan, M.; Morosuk, T.; Den, W.; Sajjad, U.; Aslam, M.M.; Farooq, M.M. Adsorption-based atmospheric water harvesting: A review of adsorbents and systems. *Int. Commun. Heat Mass Transf.* **2022**, *133*, 105961. [CrossRef]
21. Zhao, F.; Zhou, X.; Liu, Y.; Shi, Y.; Dai, Y.; Yu, G. Super moisture- absorbent gels for all-weather atmospheric water harvesting. *Adv. Mater.* **2019**, *31*, 1806446.
22. Sultan, M.; Bilal, M.; Miyazaki, T.; Sajjad, U.; Ahmad, F. Adsorption-Based Atmospheric Water Harvesting: Technology Fundamentals and Energy-Efficient Adsorbents. In *Technology in Agriculture*; IntechOpen: London, UK. Available online: https://www.intechopen.com/chapters/76511 (accessed on 14 June 2022).
23. Kode, V.R.; Stuckenberg, D.J.; Went, E.K.; Erickson, O.M.; Plumer, E. Techno-economic analysis of atmospheric water generation by hybrid nanofluids to mitigate global water scarcity. *Liquids* **2022**, *2*, 183–195. [CrossRef]
24. Siegel, N.P.; Conser, B. A Techno-Economic Analysis of Solar-Driven Atmospheric Water Harvesting. *J. Energy Resour. Technol.* **2021**, *143*, 090902. [CrossRef]
25. Adeyanju, A.A. Theoretical and Experimental Analysis of Atmospheric Water Harvesting Device. *Prog. Can. Mech. Eng.* **2020**, *3*, 1–7. [CrossRef]
26. Sibie, S.; El-Amin, M.; Sun, S. Modeling of Water Generation from Air Using Anhydrous Salts. *Energies* **2021**, *14*, 3822. [CrossRef]
27. Li, R.; Shi, Y.; Shi, L.; Alsaedi, M.; Wang, P. Harvesting Water from Air: Using Anhydrous Salt with Sunlight. *Environ. Sci. Technol.* **2018**, *52*, 5398–5406. [CrossRef]
28. Gordeeva, L.; Restuccia, G.; Freni, A.; Aristov, Y. Water sorption on composites "LiBr in a porous carbon". *Fuel Process. Technol.* **2002**, *79*, 225–231. [CrossRef]
29. Zhang, H.; Yuan, Y.; Sun, Q.; Cao, X.; Sun, L. Steady-state equation of water vapor sorption for $CaCl_2$-based chemical sorbents and its application. *Sci. Rep.* **2016**, *6*, 34115. [CrossRef] [PubMed]
30. Bhowmik, M.; Haldar, S.; Dharmalingam, K.; Muthukumar, P.; Anandalakshmi, R. Evaluation of Thermo-Kinetic and Absorption Characteristics of Pure Desiccants and Desiccant Mixtures. *Mater. Today Proc.* **2020**, *26*, 1967–1971. [CrossRef]
31. Elashmawy, M.; Alshammari, F. Atmospheric water harvesting from low humid regions using tubular solar still powered by a parabolic concentrator system. *J. Clean. Prod.* **2020**, *256*, 120329. [CrossRef]
32. Almasarani, A.; Ahmad, I.K.; El-Amin, M.F.; Brahimi, T. Experimental Investigations and Modeling of Atmospheric Water Generation Using a Desiccant Material. *Energies* **2022**, *15*, 6834. [CrossRef]
33. Milly, P.C.D. Moisture and heat transport in hysteretic, inhomogeneous porous media: A matric head-based formulation and a numerical model. *Water Resour. Res.* **1982**, *18*, 489–498. [CrossRef]
34. Zeng, Y.; Su, Z.; Wan, L.; Wen, J. Numerical analysis of air-water-heat flow in unsaturated soil: Is it necessary to consider airflow in land surface models? *J. Geophys. Res. Earth Surf.* **2011**, *116*, 1–18. [CrossRef]
35. Philip, J.R.; De Vries, D.A. Moisture movement in porous materials under temperature gradients. *Trans. Am. Geophys. Union* **1957**, *38*, 222–232. [CrossRef]
36. Saito, H.; Šimůnek, J.; Mohanty, B.P. Numerical Analysis of Coupled Water, Vapor, and Heat Transport in the Vadose Zone. *Vadose Zone J.* **2006**, *5*, 784–800. [CrossRef]
37. Solve 1-D Parabolic and Elliptic PDEs-MATLAB Pdepe. Available online: https://www.mathworks.com/help/matlab/ref/pdepe.html (accessed on 9 December 2021).